Current Medical Imaging Reviews, 2017, *13*, 364-382

REVIEW ARTICLE

Adipose Tissue Measurement Using Magnetic Resonance Imaging: A Survey

John Bliton, Daniel Sussman, Ronald M. Summers and Jianhua Yao*

Department of Radiology and Imaging Sciences, Clinical Center, The National Institutes of Health, 10 Center Dr, Bethesda, MD 20892, United States

ARTICLE HISTORY

Received: July 13, 2015
Revised: February 15, 2016
Accepted: February 15, 2016

DOI:
10.2174/1573405612666170710163051

Abstract: ***Background*:** Adipose or fat tissue measurement by MRI is a procedure that produces results similar to those of CT without exposing patients to harmful radiation.

***Discussion*:** This review explains the nature and value of adipose tissue (AT) measurements that can be performed with MRI.

***Conclusion*:** This paper attempts to provide a general understanding of the acquisition sequences and image processing methods used in measurement and analysis of body AT, as well as the validation and uses of such information. Current methods of MRI-based AT measurement are reviewed and explained in detail.

Keywords: Adipose tissue, MRI, visceral adipose tissue, segmentation, imaging sciences, radiology.

1. INTRODUCTION

Obesity has been associated with reduced longevity, increased mortality rates, and increased risk for many diseases [1]. These disorders include hypertension, cardiovascular disease, hypertriglyceridemia, high-density-lipoprotein cholesterol deficiency, insulin resistance and diabetes mellitus [2]. Investigation of obesity in children has linked it to high blood pressure, dyslipidemia, and a higher prevalence of factors associated with insulin resistance and type 2 diabetes [3]. In addition to these dangers associated with general obesity, related risks have been associated with the distribution of AT within the body [4]. For example, visceral AT is particularly strongly associated with cardiovascular disease [5] and insulin resistance, especially in patients with type 2 diabetes [6]. As obesity becomes increasingly common in affluent societies around the world, accurate and efficient measurements and localizations of AT are becoming more important, as they allow for improved quantification and staging of adipose-related disease. AT serves as a depot for the body's energy stores. AT differs from nearly all other tissue in that it consists primarily of triglycerides, or fat. Subcutaneous AT (SAT) is found between the skin and bone or muscle all around the periphery of the body. Intramuscular AT (IMAT) exists inside muscles. Visceral AT (VAT) is found within the abdomen, among the organs. Men tend to store more AT within the abdomen than women [7].

Mattsson and Thomas provided a detailed discussion of body composition measurement methods [8]. Anthropometry, direct measurements of weight, density and/or distance performed on the body, provides less information compared to imaging measurements and its accuracy can depend on many factors including age, gender, and ethnicity [9].

Hydrodensitometry is considered as the most accurate of traditional methods. It involves measuring water displacement to estimate a person's volume. The patient's volume and mass are used with estimated densities of bone, AT, and other soft tissue to compute total AT volume.

Body mass index (BMI) is one of the most common anthropometric measures in obesity research because it can be calculated using only weight and height [10]. However, BMI also suffers from considerable inaccuracies in patients with unusual body composition, even when compared to other anthropometric techniques [11].

Dual energy X-ray absorptiometry (DEXA) is a relatively accurate 2-dimensional radiological method that provides measurements of fat, bone and other soft tissue [12]. In DEXA, two X-ray sources with different energies scan the body, yielding data that can be analyzed to estimate the composition of tissue in given regions of the body.

Each of these techniques serves very well for some purposes, but none enable detailed localization of AT. However, computed tomography (CT) provides reliable, high resolution cross-sections and is now considered the gold standard for measuring AT distribution [13]. Unfortunately, CT uses ionizing radiation (X-Rays), which poses a potential cancer risk, especially to patients who will require multiple scans. Magnetic resonance imaging (MRI) technology has become popular in body composition research because it provides all the benefits of a 3D imaging medium without requiring ex-

*Address correspondence to this author at the Department of Radiology and Imaging Sciences, Clinical Center, The National Institutes of Health, 10 Center Dr, Bethesda, MD 20892, United States; Tel: 301-402-3225; E-mail: jyao@cc.nih.gov

1875-6603/17 $58.00+.00

posure to ionizing radiation. This allows for MRI to be used repeatedly in longitudinal studies and in most patient populations. Furthermore, MRI can be used to quantify the adipose content within organs such as muscle or liver [14, 15].

There has already been a number of relevant review papers published on related issues, but none on AT measurement techniques that use MRI scans specifically. For example, Vovk *et al.* [16] reviewed methods for reducing intensity inhomogeneities in MRI. Van der Kooy and Seidell reviewed methods for measurement of adipose tissue from a clinical perspective, and found that the three-dimensional imaging techniques are optimal [17].

This paper is a review of AT measurement techniques that use magnetic resonance imaging (MRI). It explains these techniques and reviews the evidence for each approach. The paper is structured sequentially just as the workflow of an AT measurement could be - Fig. (**1**) serves as an outline of both the paper and an ordinary AT measurement procedure. Section II describes the history of MRI, acquisition parameters and protocols. Image processing methods are presented in section III. Section IV explains how MRI data has been validated thus far. In the last two sections we examine the patient populations that have been studied as well as how MRI has been used to assess the risks of excess weight. Section V gives a few known applications of knowledge of AT content and distribution. Section VI presents some basic overarching conclusions and attempts to identify some valuable opportunities for future work.

1.1. Article Selection

To find the majority of the articles we cite, a PubMed search was done using the keywords "MRI or MR or (magnetic and resonance imaging) and (adipose or fat) and (visceral or subcutaneous or abdominal)." From these results, articles were selected based on their relevance to the AT measurement process using MRI. The chosen articles give a comprehensive picture of the recent developments in MRI-based assessment of adipose tissue content.

2. ACQUISITION

The first section of this part reviews the physics and history of MRI. In the remainder, we will give a survey of acquisition sequences that have been used for AT measurement. In section 2.2 we give an overview of some of the relevant properties of AT that are characterized in MR. Section 2.3 gives an overview of standard T1 weighted techniques while sections 2.4 and 2.5 discuss water suppression and Dixon sequences which were specifically developed for AT quantification.

2.1. Physics and History

MRI and other forms of Nuclear Magnetic Resonance (NMR) rely on radiation emitted when a nuclei jump from excited, unstable states to less energetic states. An NMR apparatus uses strong magnetic field (B_0) to make these two states distinct in a sample, and uses a radio frequency (RF) pulse of radiation to excite some subset of the nuclei. B_0 must be kept very consistent across space; inhomogeneities in the field lead to artifacts that will be discussed in section 3.1. The frequency of the radiation required to excite a given nucleus is specific to the nucleus and the surrounding atomic environment, particularly the electron density. This frequency is called the Larmor frequency, and the difference between a nucleus's Larmor frequency to that of a standard at the same B_0, divided by the standard, is called chemical shift [18].

When an RF pulse is applied to a sample, it changes the longitudinal component of the sample's magnetization by exciting some nuclei, such that the longitudinal components of their spin vectors align antiparallel to B_0 (like ordinary magnets, nuclei are in a lower energy state when aligned parallel to the surrounding magnetic field). Once in this state, the excited nuclei in the sample undergo an exponential decay to the stable state. The rate of this decay is called the T1 relaxation time, the time required to reduce the difference between the sample's longitudinal magnetization and its equilibrium value by a factor of *e*. RF pulses also align the transverse (normal to B_0) components of nuclear spin vectors, and the rate of decay of net transverse magnetization is called the T2 relaxation time. T2 is the time required for the transverse magnetization to drop by a factor of *e* (by roughly 63%). While T1 is first-order relaxation, T2 is cross relaxation; it is caused by changes and inconsistencies among the magnetizations of neighboring atoms [19].

Because nuclei absorb radiation and resonate at only characteristic Larmor frequencies, the Larmor frequencies and chemical shift can be used to indicate the contents of a sample. MRI was born through the work of Damadian [20], Lauterbur [21] and Mansfield [22], work that brought NMR from a single dimension into three dimensions by adding magnetic field gradients and new computational methods. Many other scientists played critical roles in the develop-

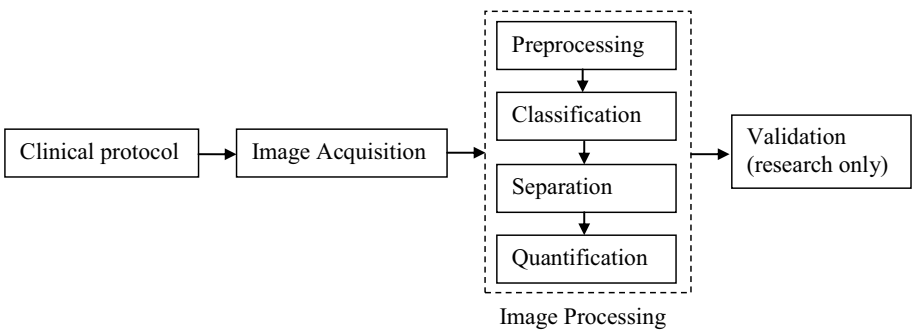

Fig. (1). Flowchart of adipose tissue measurement using MRI.

ment of MRI (Ernst and Edelstein, for example) [18], but these three have received the most recognition for MRI specifically; the latter two scientists were consequently awarded a Nobel Prize (http://nobelprize.org/nobel_prizes/medicine/laureates/2003/). For a more detailed description of the history and physics of MRI, see Hornak's hypertext textbook [18].

2.2. Tissue Properties

The hydrogen atoms in triglycerides have, on average, characteristic T1, T2 and chemical shift values. Though these values will vary considerably and may overlap with those from other tissues, they usually make it possible to distinguish AT regions from other tissues. Chemical shift, T1 and T2 relaxation times depend on tissue composition, magnetic field strength and temperature [23]. AT has shorter T1 and T2 relaxation times than practically all other normal tissues [24]. Also, with increasing field strength, T1 for water-based tissue increases faster than for AT [25]. T1 relaxation times for AT are generally consistent across age, gender, weight, health conditions, and anatomical region [26].

2.3. T1-weighted Acquisition Sequences

T1-weighted scanning sequences make relative intensities of tissues in a MRI scan depend on their T1, creating contrast between AT and other tissues. These sequences use short TR and TE to increase signal intensity as T1 shortens [27]. Common sequences to generate T1-weighted images are spin echo (SE) and gradient echo (GE). Variants of GE include spoiled GE, steady state GE, and balanced GE [28]). Inversion recovery (IR) can be applied to prepare the sequence [29].

SE and its variants have been used frequently for AT measurement. For example, Staten *et al.* [30] and Lancaster *et al*. [27] used SE in their early studies, while Seidell *et al.* [31] and Sobol *et al.* [32] used IR and validated the technique against CT measurements. Terry *et al.* [29] compared IR and SE sequences, and noted that SE is more likely to be used for an AT measurement protocol (see Table **1**).

2.4. Water Suppression Techniques

Water suppression techniques attempt to actively reduce signals from protons in water molecules, while leaving AT signal unaltered, thereby increasing contrast between AT and most other tissues. For example, selective excitation uses a series of RF pulses that use certain flip angles such that only AT molecules are given transverse magnetization [33]. Another strategy is water saturation, which uses selective RF pulses to excite water such that its signal can eventually be selectively eliminated [34].

Table 1. Summary of acquisition methods. The first author and the publication year are given. Number of subjects (N), slices and scanning region are given. The pulse sequence is described. Standard scanning parameters TR (repetition time), TE (echo time), field strength, flip angle, FOV (field of view), total scan time and matrix dimensions are given for the studies that published them. Blank entries in the table indicate that the information was not provided in the paper.

First Author	Year	N	Slice Num	Region	Description	TR (ms)	TE (ms)	B_0	Flip Angle	FOV (cm)	Scan Time (s)	Matrix
Staten [30]	1989	6	3	Chest, abd, thigh	Spin echo	500	17	0.5	-	50	-	256x256
Lancaster [27]	1990	35	4	Abdomen	T1-weighted spin echo	500	20	1.5		32-48	75	256x256
Seidell [31]	1990	7	6	Abdomen	Inversion recovery: 300ms inversion time	820	20	1.5	-	45	100	128x256
Fowler [89]	1991	14	17	Whole body, phantoms	Inversion Recovery Pulse Sequence	370	170	0.1	-	-	47	-
Gerard [100]	1991	9	21-24	Abdomen	T1-weighted spin echo	400	20	0.6				
McNeill [96]	1991	14	28	Whole Body	Fast inversion recovery			0.1			47	
Sobol [32]	1991	18	7	Abdomen	Water suppression, inversion recovery (TI=300ms)	800, 833	30, 30	1.5	-	40-45	-	-
Ross[65]	1992	17 rats	42		Spin-echo, use oil tubes for calibration	500	20	1.5	-	-	119	256x256
Abate [63]	1994	3	3	Abdomen	T1-weighted spin echo	300	15	0.4	90	51.2x 38.4	-	256x192
Terry [29]	1995	158	4,1	Abdomen	Inversion recovery, spin-echo	833, 100	30,30	1.5	-	-	-	256x256
Barnard [28]	1996	9	1	Abdomen	RF spoiled gradient echo, steady-state free precession, T1-weighted spin echo, Rapid T1-weighted spin echo.	9, 33, 500, 36	4, 8, 20, 14	1	40, 90, 90, 120	60	4.1, 1.8, 768, 3.9	192x256

(Table 1) Contd…

First Author	Year	N	Slice Num	Region	Description	TR (ms)	TE (ms)	B_0	Flip Angle	FOV (cm)	Scan Time (s)	Matrix
Elbers [85]	1997	30	1,3	Abdomen, whole body	Inversion recovery, 6 repetitions	524	24	0.6	-	-	-	256x256
Han-McNeill [64]	1997	20	4	Abdomen	Inversion/saturation recovery	1000	-	0.1	-	-	-	-
Han-Kelly [66]	1997	23	4	Abdomen	Spin Echo	350	12	1.5	-	-	-	-
Gronemeyer [62]	2000	16	31	Abdomen	T1-weighted spin echo	700	15	1.5	90	50	720/1440	128x256
Donnelly [48]	2003	NA	N/A	Phantom Abdomen	Spin echo, 3D spoiled gradient-echo, fast Dixon	500, 5.5, 500	14, 1.6, min full	1.5	-	-	150, 15, 330	256x160, 128x128x26
Jin [87]	2003	2	6	Abdomen	T1 weighted (data produced in different study)	-	-	-	-	-	-	-
Poll [118]	2003	37	4	Abdomen	T1-weighted spin echo	389	14	1	-	40-50	420	256x154
Positano [60]	2004	20	32	Abdomen	T1-weighted fast gradient-echo (GE FIESTA)	120	4.2	1.5	90	36-48cm	-	256x256
Tintera [33]	2004	14	21	Abdomen	Turbo spin-echo w/water suppression, turbo factor 5	200	12	1.5	-	42-45	11	-
Brennan [59]	2005	42	Patient-specific	Whole body	T1-weighted gradient-echo	112	1.62	1.5	70	-	-	256x256
Tatsuya [75]	2005	11	1	Abdomen	Dual echo spin echo	200	15.5, 26.9	0.3	-	30-34	30	160x152
Machann [68]	2005	60	100-130	Whole body	T1-weighted spin echo	490	12	1.5			12	256x178
Peng [35]	2005	6	6	Abdomen, Phantom	T1-weighted turbo spin echo (turbo factor 7), water saturated 3d balanced steady-state free precession (ETL=128)	500, 2.9	5, 1.2	1.5	90, 55	40-50	4.7, 1.8	256x256
Armao [34]	2006	5	40-45	Abdomen	Conventional T1-weighted spoiled gradient-echo, T1-weighted spoiled gradient-echo water-saturation	285, 285	4.4, 1.61	1.5	90	40	60	154x256
Kullberg [127]	2006	10	150	Whole body	T1-weighted gradient echo sequence, two with RF power and receiver optimization and noise determination turned off	177	2.3	1.5	80, 80, 30	53	-	-
Liou [70]	2006	39	15	Abdomen	T1-weigted spin-echo; T1 weighted fluid attenuated inversion recovery; short inversion time inversion recovery; t2-weighted fast recovery fast spin-echo	-	-	1.5	-	44x44	-	512x512
Arif [124]	2007	10	10	Abdomen	T1-weighted multislice spin echo inversion recovery	550	12	1.5	-	50x50	-	256x256
Bonekamp [119]	2007	15	8	Abdomen	T1-weighted spin echo	150	4.6	1.5	-	53x53	-	256x256

(Table 1) Contd…

First Author	Year	N	Slice Num	Region	Description	TR (ms)	TE (ms)	B_0	Flip Angle	FOV (cm)	Scan Time (s)	Matrix
Demerath [128]	2007	40	21-35	Abdomen	T1-weighted fast-spin echo pulse sequence	322	12	1.5	-	48x36	-	
Peng [69]	2007	6	8	Abdomen, phantom	Water-saturated balanced steady-state free precession	3.6	1.36				17	400x400
Tanaka[36]	2007	14	50	Abdomen	WSPIR, WSPAIR	3.9	1.9	1.5	5	-	-	-
Leinhard [49]	2008	18	1	Abdomen	Dual echo, multi slice, spoiled, fast gradient echo pulse	286	2.3, 4.6	1.5	80	29x41x20	-	-
Li [37]	2008	10	1	Abdomen	Fast spin echo; water suppressed fast spin echo, breath hold, echo train length	333	13.1	3	90	-	-	256×192
Positano [74]	2008	20	32	Abdomen	T1-weighted spin echo pulse	500	12	1.9	-	-	-	-
Gensanne [126]	2009	30	5	Thigh, Phantom	T2 multi-spin echo sequence, 16 echoes	2000	22.5	1	-	25x25	-	-
Kullberg [71]	2009	10	28	Whole body	T1-weighted gradient echo sequence, two with RF power and receiver optimization and noise determination turned off	177	2.3	1.5	80, 80, 30	53	-	-
Kullberg [58]	2009	24	Patient-specific	Whole body	Combine water+fat, sample 3 gradient echoes after [ulse, images reconstructed to water and fat and B0 inhomogeneity	5.9	1.36/2.22/5.09	1.5	3	53x37.7	-	-

Many groups have put forward valuable water-suppression methods. Tintera *et al.* [33] describe a AT measurement protocol that uses a modification of the turbo SE sequence to create images with fat-to-muscle contrast that was on average four times as high as in standard images. Armao *et al.* [34] showed that a water saturation technique reduced standard deviations among repeated measurements on the same image from 26% to 2%. Peng *et al.* [35] used a modification of the balanced steady-state free precession sequence to suppress water signal. When compared to SE sequences, the sequence significantly increased the contrast-to-noise ratio between AT and three other areas: Muscle, large bowel, and small bowel. Tanaka *et al.* [36] compared two water-suppressing variations on the inversion recovery sequence, and determined that their spectral presaturation with inversion recovery (SPIR) sequence gave the maximum amount of AT. Li *et al.* [37] compared reproducibility between standard fast SE and water suppressed fast SE. They found that water suppression reduced the coefficient of variation (CV) of the VAT/TAT ratio from 19.2% to 5.2% and had good reproducibility for SAT, VAT and girth measurements.

2.5. Dixon Methods and Fat-water Separation

Dixon methods differ from the above methods in that, rather than modifying the RF pulses or magnetic field, they manipulate the timing of image acquisitions. The timing is tuned such that two data sets are created, one called "in-phase" and one called "opposed". The magnetizations of most adipose protons (CH_2) are parallel and antiparallel to those of water protons in the in-phase and opposed data sets, respectively. In the presence of a completely uniform B_0, the sum of the in-phase and opposed images creates the "water" image and the difference between the images creates the "fat" image [38]. Unfortunately, B_0 is never completely homogenous, and small inhomogeneities greatly reduce the functionality of the original Dixon methods. Dixon's original method, a "two point" method, required only two images because it assumed that the sample's magnetization was the only factor affecting the signal. Most modern techniques use an additional acquisition or an additional "point" to account for B_0 inhomogeneity, though modifications can be made to two-point methods to accomplish the same goal [39]. The additional-image approach [40] and three point method [41] are both means used to correct for B_0 field inhomogeneity, and many studies correct for the B_0 field inhomogeneity in these ways [39, 42, 43]. Also, some methods reconstruct the fat and water images from a single acquisition [44]. Dixon methods have sometimes been shown to be prone to error because the small differences in chemical shift among lipids can result in the estimated AT signal's leaking into the estimated water signal [45]. However, Moriguchi's group has

developed methods to help correct for variance in the signal from AT [46, 47].

Dixon-based methods have been used less than rival methods in AT measurement studies, possibly because they are not as well-known or because early studies found poor correlation between AT measured in Dixon fat images and CT images. Donnelly *et al.* [48] compared a new Dixon sequence to spin-echo and 3D spoiled gradient-echo, when measuring AT in an abdominal phantom. The Dixon method consistently provided volume estimates which were closest to the true volume for phantom SAT and VAT, increasing the volume estimates from 86.5% to 94.7% and 62.3 to 69.7% of the true volume, respectively. Leinhard [49] used a Dixon method when creating an automated segmentation algorithm which used phase information for inhomogeneity correction and registration. Dixon methods are favored to quantify fat in livers and other organs where adipose tissue is a smaller percent of each voxel, because Dixon methods can be used to quantify the amount of AT in each voxel [50]. Yu *et al.* [51] combined Dixon methods with region growing algorithm and improved rates of false positives relative to an approach without region growing.

2.6. Table 1 Summary

Table **1** lists some (44) of the reviewed papers regarding the acquisition methods. Most studies were small; the number of subjects in the study ranged from 4 to 158, with an average of 24 and a median of 20. The number of slices ranged from 1 to 150, with a mean value of 21, though most experiments used less than 20 image slices, in particular those that scanned only the abdomen. T1-weighted spin echo sequences were the most common, though gradient echo and inversion recovery sequences are also present. Most of the papers reported B_0, the repetition and echo times, but much of the remaining information about the scanning procedures is missing. For a detailed explanation of the technical parameters of MRI, see [18].

3. IMAGE PROCESSING METHODS

In this section, we present the image processing methods to quantify AT and AT distribution. This is divided into four main parts: (1) image preprocessing, (2) AT classification, (3) SAT and VAT separation, and (4) AT quantification. Fig. (**2**) gives an example of an AT segmentation that uses some of the methods discussed here and those in Section 2.

3.1. Preprocessing

In this section, we will focus on methods that correct for intensity inhomogeneities or bias fields, which are present in almost all MRI images. First, though, we will briefly discuss techniques for noise reduction in images.

Noise reduction strategies are rarely reported in AT measurement papers, though they have been used in some studies. Three of such exceptions are the work of Barnard *et al.* [28], Sussman *et al.* [52] and Al-Attar *et al.* [53]. Barnard *et al.* used a speckle filter to reduce noise while Sussman *et al.* applied an anisotropic diffusion filter. Al-Attar *et al.* used an "auto brightness" tool to reduce noise in the background.

Intensity inhomogeneities are artifacts specific to the MR medium. They result from imperfections in the gradient field of the magnet as well as perturbations of the field by the body. In practice, a bias field causes the intensities of very similar tissues to vary across the image, which can lead to incomplete segmentations or leaks. Like artifacts in general, this means that areas of adipose tissue will not be recognized as such, especially by an automated algorithm, and that non-adipose tissue could be mistaken for adipose tissue. Because the bias field can be different for each scan, it is often difficult to measure the fields, and they are usually estimated based on other assumptions.

One technique for estimating these fields is a type of expectation-maximization (EM) process. For AT measurement, one first creates a preliminary AT segmentation. These voxels are all assumed to be AT, such that they should all have the same intensity in an ideal image. The bias field is estimated by calculating a ratio between the intensity of the voxels on the surface of these segmentations and the mean value of all of the voxels.

Many groups have used this approach. Kullberg *et al.* [54] marginally improved their results by fitting a quadratic surface to threshold based segmentation. Jørgensen *et al.* [55] found local maxima and fit thin plate splines to generate a surface. These techniques are fast and improve results if the bias fields are very smooth and are not very strong. On stronger bias fields, especially where some areas are visibly darkened, these techniques will not work as well because the darkened AT will not be included in the initial segmentation.

A different technique, non-parametric non-uniform intensity normalization (N3) attempts to correct for intensity inhomogeneities by maximizing high frequency components of

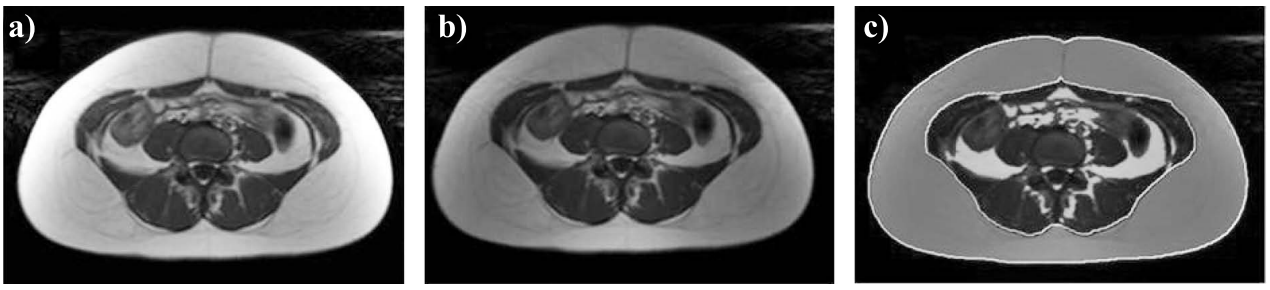

Fig. (2). Example of T1 weighted MRI and AT measurement. **a**) T1 weighted MRI of abdomen. Scanner: Philips Achieva 1.5T, Sequence: SE, TR:400, TE:8, Flip Angle: 90; **b**) Inhomogeneity correction for image preprocessing; **c**) AT pixel classification and VAT and SAT separation. Red: SAT, Green: VAT. *(The color version of the figure is available in the electronic copy of the article).*

the image histogram [56]. Sussman *et al.* [52] used this technique, and Tustison and Gee [57] developed a variation of it.

In addition to image processing techniques, acquisition sequences can be tuned to correct for intensity inhomogeneities. Dixon acquisition sequences generate multiple images by leveraging the phase differences between AT and water (see section 2.5). These images can also be used to approximate field inhomogeneities. Kullberg *et al.* [58] used a 3-point Dixon method to perform such a correction.

Many other tools exist to perform intensity inhomogeneity corrections in both 2D and 3D images. Brennan *et al.* [59] used histogram matching to correct inhomogeneities that occur across axial slices. Barnard *et al.* [28] used a low-frequency reconstruction to correct bias fields using frequency information. For a more detailed overview of intensity inhomogeneity correction techniques see Vovk *et al.* [16]. By far, there is no perfect method for artifact correction since the artifact is somewhat random and affected by many factors. However, all the reviewed methods alleviate the intensity inhomogeneity and generate more consistent images for following processing.

3.2. AT Classification

Classification of AT is the process of deciding which voxels in the image correspond to AT. As noted in Section 2, images acquired for the purposes of AT measurement will have far higher signal intensities from AT than from most other tissues, though some other regions (especially iron-rich regions) will also have very high intensities. We will discuss three kinds of methods for making this selection: Manual tracing, thresholds, and more advanced techniques such as fuzzy c-means [60], fuzzy connectedness [61], and region growing [62].

Manual tracing has been used in multiple studies and usually demonstrates a high accuracy [63, 64]. While this method works best for classifying large connected depots, its greatest drawback is the cost in time to users, and simple segmentations require little.

Threshold methods require that AT voxels be brighter than other voxels in the image. In general, some method is used to select an intensity threshold, t, and any voxels above t are labeled as AT and all others are labeled as non-AT. Some scientists have tried use fixed thresholds by using sets of training images to produce a fixed threshold, but these studies were designed to test other parts of their methods and using fixed threshold is unlikely to work unless the imaging protocol is held constant [65, 66].

Histogram-based methods use information from the images' gray-level histograms to choose a threshold. Gray-level histograms show the distribution of voxels' signal intensities, seen as shades of gray. Ideally, there would be a narrow peak for AT and a broader peak for most other tissues, but these peaks are not always distinct. In most cases the histograms are calculated from the entire image, but histograms along contours near the body boundary have been used as well [67].

Some researchers have used the mid-point between the tissue peaks [27, 31] as a threshold while others have used the minimum point or valley between the peaks [37, 68]. For images where there is little or no signal from water, a threshold can be selected at half the intensity of the AT peak [58, 69]. These histograms come from water-suppressed images in which the water peak occurs near zero intensity. The selection of half the AT peak allowed Peng's group to account for voxels with only a partial volume of AT, though this approach assumes that there is very little signal from non-water, non-adipose hydrogen [69].

Standard statistical threshold selection techniques have also been used. Liou *et al.* [70] used Ridler and Calvard's iterative method and Kullberg *et al.* [71] used Otsu's method, which minimizes intra-class variance (or equivalently, maximizes inter-class variance) [72]. Also, a Gaussian may be fit to each peak, in which case a typical threshold selection would be the intersection of the two distributions, the minimum between the peaks [73].

Some image processing techniques do not rely solely on intensity thresholds. Fuzzy c-means (FCM) is an unsupervised classification method that iteratively estimates centroids for each class and then, based on those centroids and voxel intensity, calculates fuzzy membership maps for the image. Though FCM suffers from problems with inhomogeneities, Positano *et al.* have integrated spatial constraints into the fuzzy c-means algorithm to help correct for intensity inhomogeneities [74].

Due to the inconsistency of MR images, there is no constant threshold for AT classification. The thresholds are often needed to be decided on study-basis. Therefore, supervised or unsupervised clustering techniques can generally produce better results.

3.3. Separation of SAT and VAT

Generally, separation of SAT and VAT depots is carried out following the classification step, though some methods perform these step simultaneously. We first discuss the manual techniques such as labeling and contour drawing. We then discuss automated methods.

One manual technique is to draw contours that separate the AT depots. In some cases, one contour is considered sufficient to separate SAT and VAT [30, 31, 75] but usually, one contour serves to segment the body from the image background and the second contour separates the SAT and VAT depots [33, 69, 73].

Contours may also be created automatically or semi-automatically using computer algorithms. An overview of these and related methods is provided by He *et al.* [76]. These algorithms use image properties in conjunction with other factors built into the algorithm to automatically find a desired contour. Active contour models (ACM) are common variants of contour-based methods [77]. ACMs function by iteratively applying forces to a contour. The forces drive control points or vertices towards edges of sections in the image An example of an additional force is the balloon force proposed by Cohen *et al.* [78], which serves to either inflate or deflate the contour. ACM has been used to separate SAT from VAT by driving an initial subcutaneous contour near the body boundary towards the subcutaneous fat-muscle boundary in the abdominal wall.

Another approach is contour following, which traces the border between AT and other tissues starting from one or more seed points (the use of seed points distinguishes this from edge detection) [67]. Livewire is an example of this kind of approach [79]. Others have used dynamic programming to find contours in images that are converted to polar coordinates [55, 80]. Other contour-based methods such as graph cut and level set [81] exist, but many have yet to be used in AT measurement algorithms.

Knowledge-based methods use either *a priori* assumptions about the body or information from other previously segmented images. For example, in Kullberg [54], the method consisted of first finding the spine and then modeling the pelvis as a v-shape. The spine was identified by finding a translation of a template that minimizes the difference between the template and the image. Using the information about the pelvis, the researchers created bounds beyond which tissue could not be called AT [54].

Active shape modeling is another knowledge-based method, where prior segmentations of the abdomen are used to segment new images. First, prior images are annotated with landmark points and information about these points is used to align prior images to the current image. This process has been used to segment VAT and SAT and create three boundaries: one around the body, one along the deep surface of the subcutaneous AT, and one enclosing the VAT [55]. Active appearance models have also been proposed to employ both the shape and texture properties in the segmentation [82].

For organ specific AT measurement, the organs are often needed to be segmented first. Statistical shape models [83] and atlas based techniques [84] have been widely studied for organ segmentation.

3.4. Simultaneous Classification and Separation

Region-growing algorithms are used to classify and/or separate regions by starting at a seed point and propagating the region outward based on some affinity criterion. These seed points may be chosen manually [34, 62, 85], or they may be based on a given threshold [59]. Region-growing methods usually classify connected voxels based on their intensity relative to their neighbors, rather than using some image-wide standard. This allows the algorithm to propagate through smooth inhomogeneities and still stop properly at region boundaries. Region growing is good for segmenting SAT because SAT is a coherent whole, though region-growing can leak into VAT depots.

Fuzzy-connectedness [86], another variant of region growing, generates affinity relationships between one or more seed points and the remaining image. Udupa *et al.* [86] designed the fuzzy-connected region growing algorithm, which generates a fuzzy affinity map showing the affinity between a voxel and a starting seed. A threshold can then be applied to this fuzzy connectedness map to attain a segmentation of SAT [53, 87]. Roullier *et al.* [88] also used fuzzy clustering and fuzzy connectedness algorithms to measure AT.

3.5. Quantification

The final step is to quantify the amount of AT in each class and depot. Quantification entails counting the number of voxels that fit into each class and then converting these totals into meaningful measurements.

Some voxels will inevitably contain significant fractions of both adipose and non-AT, such that they are difficult to classify. This leads to a partial volume effect, which can be partially dealt with using a histogram-based quantification that does not require voxel-by-voxel classification [27, 60, 74].

MRI data is reconstructed in slices and assumptions must be made to account for the volume between slices. The truncated cone model [64, 89], the truncated pyramid [65], and the two-column model [90] are methods that make assumptions to estimate the content of the inter-slice tissue. Shen *et al.* [90] found that the two column model is more accurate than the truncated cone model.

Given volume, the mass of the AT can be calculated using knowledge about its density. Because the relative concentrations of water and lipid in AT vary considerably across individuals, there is a range of densities that could be used to calculate the mass of the AT given the volume [91]. One commonly cited density is around 0.91 g/cm [3, 59]. Some have used this density to calculate the mass of the triglycerides that make up approximately 80% of AT [63, 64, 66]. Others have reported the 80% triglyceride figure for volume calculations as well [67], though the range identified by Martin *et al.* is 54-85%. Martin *et al.* also found that an individual's overall obesity may predict his or her actual lipid concentration [91].

3.6. Table 2 Summary

Table **2** summarizes a few (36) of the reviewed papers regarding the image processing methods for AT measurement. Among the categories of automation, the papers given are roughly evenly divided; 8 used manual methods, 10 used semiautomatic methods and 9 used completely automatic methods. 9 studies used some kind of preprocessing, and all but one of these used entirely automatic methods (the remaining one used a semiautomatic method). From 1989 to 2010 there is a clear trend toward the use of automatic techniques for classification of adipose tissue. The use of simple classification thresholds is becoming less common among researchers as they develop more accurate and delicate methods. VAT/SAT separation is also being performed with more automation based on a variety of mathematical techniques. The trend is not as stark as for classification.

4. VALIDATION

In this section we give an overview of how AT measurement techniques have been validated and how performance is measured. This section is divided into five subsections. The first section gives a brief overview of the statistical methods that can be used to compare two measurements and validate the measurement against ground truth. The following four sections describe four approaches to MR AT measurement validation: (1) Phantoms, (2) Non-Imaging techniques, (3) Non-MR imaging techniques, and (4) Other MR techniques.

Table 2. Summary of image processing methods. The first author and year are provided to identify the study. The degree of automation is described. Preprocessing procedures are indicated, followed by short descriptions of classification and separation methods. Not all papers in this review used classification, and not all that did so also attempted separation.

First Author	Year	Automation	Intensity Correction & Pre-processing	Classification	VAT/SAT Separation
Staten [30]	1989	N	N	Manually selected threshold	Manual contours, 1 contour between SAT and VAT
Lancaster [27]	1990	Semi	N	Valley threshold and midpoint threshold for VAT. SAT between contours	Manual contours, draw 2 contours around SAT. 1 contour around VAT
Seidell [31]	1990	N	N	Midpoint between peaks from histogram of 3 manually drawn ROIs	Manual contours, 1 contour between SAT and VAT
Fowler [89]	1991	Semi	N	Manual thresholds	Automatic outlining, manual adjustments
Sobol [32]	1991	N	N	Manual threshold	Manual contours
Ross [65]	1992	N	N	Fixed thresholds determined from phantom with manual adjustments	Manual assigning of depots
Abate [63]	1993	N	N	Manual contours	Manual assigning of depots
Barnard [28]	1996	Semi	Y: Low spatial frequency reconstruction, speckle filter	Histogram and noise based threshold, manual adjustments	Manual contours
Han-Kelly [66]	1997	N	N	Fixed thresholds determined from phantom	Manually placed oval lines
Han-McNeill [64]	1997	N	N	Manual contours	Manual assigning of depots
Thomas [67]	1998	Semi	N	Thresholds based on histogram statistics and noise calculations	Contour following, shape constraints for bone ID, knowledge base (atlas) to extract VAT boundary, manual refinement
Gronemeyer [62]	2000	Semi	N	Manual: "magic wand" used to outline fat depots. Semiautomatic: Erased intra-abd. tissue, selected threshold to find SAT; used same threshold on whole image to find TAT	Erase intra-abdominal tissue to get SAT. Restore for VAT
Jin [87]	2003	Y	N	Fuzzy connectedness for SAT; Vornoi Diagram homogeneity classifier for VAT	Fuzzy connectedness for VAT, level set based volume preserved smoothing
Poll [118]	2003	Semi	N	Fit two Gaussians to histogram; use min between Gaussians	Manual contours, 2 contours, 1 around body, 1 between SAT and VAT
Positano [60]	2004	Y	N	Fuzzy C-means	Active contour models
Tintěra [33]	2004	N	N	Min between noise voxels and fat peak (water suppressed scan)	Manual contours, 2 contours, 1 around body, 1 between SAT and VAT
Brennan [59]	2005	Y	Histogram matching	End of soft tissue peak, boundary refinement, region growing and refinement	None
Tatsuya [75]	2005	N	N	Manual threshold	Manual contour along medial margin of abdominal wall
Machann [68]	2005	Semi	N	Automatically set to nadir of AT peak, minor manual adjustment	Manual contours, 2 contours between SAT and VAT to exclude IMAT
Al-Attar [53]	2006	Semi	Auto brightness to minimize background noise	Threshold on connectedness map generated from manually selected seed point by connected threshold grower	None

(Table 2) Contd…

First Author	Year	Auto-mation	Intensity Correction & Pre-processing	Classification	VAT/SAT Separation
Armao [34]	2006	Semi	N	Manual thresholds	Fuzzy-connectedness to extract SAT
Liou [70]	2006	Y	N	Coarse threshold, morphological refinement,	Refine body boundary with polar coordinates polynomial fitting, use morphological distance to get VAT mask
Tanaka [104]	2006	N	N	Manual threshold	Manual
Kullberg [43]	2007	N	N	Manual contours	Manual Contours
Kullberg [54]	2007	Y	Y: Fit quadratic surface to coarse AT segmentation	Gaussian fitting if biomodal, Otsu threshold selection on SAT otherwise	SAT separation using gradient magnitude mask. Vertebra, pelvis and geometric models used to eliminate unwanted voxels in VAT. Region Growing
Peng [69]	2007	Semi	N	1/2 AT peak intensity, accounting for partial volumes	Manual contours, 2 contours, 1 around body, 1 between SAT and VAT
Leinhard[49]	2008	Y	Y: Use Dixon based techniques	Thresholding on corrected fat image	Morphological registration based on a manually segmented prototype, used to label as VAT, non-visceral internal VAT, or SAT
Li [37]	2008	Semi	N	Min between 2 peaks, manually remove unwanted voxels	Draw ellipse surrounding body, use binary threshold image to get VAT mask
Positano[74]	2008	Y	Y: Background defined by 3 class FCM	Modification of Positano 2004; spatial constraint was included in FCM to correct inhomogeneities.	Active contour models
Kullberg [71]	2009	Y	Y: Use Dixon based techniques	Threshold at 50% on fat fraction image	Use water image and knowledge base to find VAT mask, use knowledge base to exclude spine, segmented on sum image, and pelvis
Kullberg [58]	2009	Y	Y: Fit thin plate splines to sampled local maxima	3 class fuzzy c-means to cluster into AT, non-AT and background.	Active shape models, dynamic programming to find contours, set and connectivity operations
Sussman [52]	2010	Y	Y: N3 Inhomogeneity	Fuzzy C-means	Active contour models

4.1. Statistical Methods

When ground truth is known it is common to report the accuracy of the method in terms of percentage identity to the known measurement. Often the percentages for false positives, false negatives, and true positives are reported, allowing for specific quantification of how much segmentation got right and how much it got wrong. A common measure of the relationship between two data sets is the correlation coefficient [92]. A variant is the non-parametric Spearman rank correlation coefficient which measures the agreement between the rank orders of a paired set of measurements [93]. When evaluating repeated measurements, the coefficient of variation, which is the ratio between standard deviation and the mean of repeated measurements, is often given. Bland-Altman plots show the difference between two measures on the vertical axis and their average on the horizontal axis [94]. Comparing two or more Bland-Altman plots allows for analysis of which pairs of methods provide better agreement.

4.2. Dissection and Phantoms

Using phantoms or cadavers is one way to validate an MR measurement. Abate *et al.* performed a validation study which compared MR AT measurements to measurements from dissection on three cadavers [63]. AT can be simulated in phantoms with vegetable oil [35, 69], cream [48], or a solution which is meant to have similar T1 time as AT [89]. Fowler *et al.* [89] also used fresh fat and muscle in a layered phantom. Yoon [95] compared CT and MRI measurements of phantom and human scans.

4.3. Non-imaging Measurement Techniques

Relative to most imaging techniques, non-imaging techniques are usually faster and cheaper to perform. Hydrodensitometry is the most accurate of the non-imaging techniques and has been used as a validation technique in multiple MR fat measurement studies [96]. Fowler *et al.* reported volumes AT within 5% of hydrodensitometry measurements and found that MR was the best predictor of hydrodensitometry

measurements as compared to four other techniques: skinfold thickness, whole-body counting, isotopic water dilution and tetrapolar bioelectric impedance [89]. Aristizabal *et al.* [97]attempted to validate skinfold thickness measurements and found that they performed poorly.

Bioelectrical impedance is another common technique. Ward *et al.* [98] and Yoneda *et al.* [99] explored the value of bioelectrical impedance in detail. Techniques including isotopic water dilution [95, 100] and 40K whole-body counting [89] have also been used in comparative studies. A summary of techniques for measurement of visceral fat as of 1993 is given in van der Kooy *et al.* [17], and a similar summary of measurements of abdominal AT is given by Srdic *et al.* [101].

4.4. Non-MR Imaging Measurement Techniques

CT is the primary imaging method that has been used to validate MR AT measurement methods, though DEXA is also used frequently. DEXA can be used to measure fat, but cannot separate VAT and SAT as can CT and MRI. Seidell *et al.* [31] and Sobol *et al.* [32] performed two early studies that validated manual MR techniques against CT. Kamel *et al.* [7] used DEXA to validate intra-abdominal AT measurements and found relatively high levels of correlation [7] and Kullberg *et al.* [71] compared DEXA, MRI and CT, also finding very high correlations.

4.5. MRI Measurement Techniques

Comparison and evaluation of reproducibility between two acquisition sequences can be done by repeated measurements on the same image [34] or repeated acquisitions in the same slice area [71]. Another evaluation method is to compare image properties such as signal–to-noise and contrast-to-noise ratios across different acquisition sequences [70]. Elbers *et al.* [85] and Machann *et al.* [68] used repeated acquisitions with the same sequence parameters at the same location to evaluate overall reproducibility.

Many studies compare two methods of segmenting AT. Two techniques have been compared using the statistical techniques described above, including: correlations [55, 60, 74], accuracy [62, 87], coefficients of variation [27, 54] and Bland-Altman plots [52, 55, 60, 74]. Gronemeyer *et al.* [62] also used a Student's t-test to show that two methods gave significantly different results. Jin *et al.* [87] used an average of 16 segmentations by 6 raters as a "ground truth" to compare to a manual segmentation [91]. Both inter- and intra-observer reliability measurements have been reported in reproducibility studies (see Table **3**).

Table 3. Summary of validation methods and performance. The first author and the year identify the paper. The degree of automation is indicated followed by a short description of the data used. The validation techniques are described and the results are summarized. Not all papers in this review attempted validation.

First Author	Year	Auto	Subject Data	Validation Technique	Results/Performance
Staten [30]	1989	N	6, 3 male, 27-76y, BMI 18-39	Against hydrodensitometry and anthropometry	High correlations between MRI TAT and hydrodensitometry. High correlations with VAT and total body weight and waist to hip ratio
Lancaster [27]	1990	N	35 (17 obese)	20 repeated area measurements of 3 ROIs on 1 patient.	CV 1% for ROIs, 3% for SAT. Slice thickness->little significance. No significance between measurements.
Seidell [31]	1990	N	7 (4M), age 22-42, BMI 22±1.7	Against CT.	Intra-class r = 0.985, 0.791, 0.996 (TAT,VAT,SAT). Spearman r = 0.929, 0.893, 0.964 (T,V,S). Reproducibility CV 5.4, 10.6, and 10.1% (T,V,S)
Fowler [111]	1990	N	Phantom	Accuracy against known areas and volumes. Layered fat and muscle phantom.	Error of -5.7±1.3% against uniform phantom. Reproducibility: 4.3±2.7%. MRI underestimated fat mass on layered phantom.
Fowler [89]	1991	N	14, 7 normal BMI, 7 high BMI	4 repeated measurements. Against skinfold thickness, underwater weighing, 40K whole-body counting, isotopic water dilution, and tetrapolar BIE	Total volume within 5% of UWW. Other methods closer to MRI than to each other. MRI *vs.* mean of remaining methods gives r=.99. All correlations r>.85. MRI best predictor of UWW.
Gerard [100]	1991	N	9 women (5 athletes).	Repeated Measurements. Compared to D2O dilution and Bioelectric impedance	CV for reproducibility 3% SAT, 9% VAT. D2O *vs.* MRI:(Correlations: body fat percentage: r=.91, SAT percentage r=.92, VAT r=.72)
McNeill[96]	1991	N	14 females (7 overweight), Age 37±13	Compared skinfold thickness, UWW, 40K whole-body counting, BIE, MRI, body water dilution.	UWW-MRI 2.3±2.9%(SD). MRI: Smallest limit of agreement but a larger bias compared to all but body water dilution.

(Table 3) Contd…

First Author	Year	Auto	Subject Data	Validation Technique	Results/Performance
Sobol [32]	1991	N		Compared 2 MRI sequences against each other. 1 MRI sequence against CT and anthropometry.	Correlations *vs.* CT, IAAT, SAT, VAT/SAT: r=.93, .98, .81. Comparison of 2 MRI methods .92, .99, .91. Significant correlations SAT v. BMI and IAAT v. BMI.
Ross-Léger [65]	1992	N	17 rats	Compared against anthropometry	Correlations between 1 slice volume and whole volume and against anthropometry
Abate [63]	1994	N	3 cadavers. SAT, intra- and retroperitoneal AT	Against cadaver. 5 repeated measurements.	MRI-Dissection: .076±.071(SD)kg. CVs from 0.4-13.7% for IPAT and RPAT. <9% for IPAT+RPAT.
Barnard [28]	1996	Semi	9 healthy	2 repeated measurements and 2 different acquisition sequences	Mean differences of 4.7% for TAT, -1.7% for VAT between repeated measurements
Elbers [85]	1997	N	39 young, non-obese, whole body	Reproducibility of image analysis in 30 subjects, of acquisition in 9. Many comparisons	Intra-observer CV: 2.1-3.8 for abdominal, hip and thigh SAT, 9.4-13.8% for VAT. Inter-observer CV: 3.0-4.9 for abdominal, hip and thigh SAT, 11.2-17.6% for VAT. Acquisition CV: .8, 1.8, 8.4 for TAT, SAT, and VAT.
Ohsuzu [129]	1998	N	8 CT and MRI +8 MRI. Mixed sex	CT and reliability of repeated measurements	SAT, TAT, VAT/SAT : r=0.93, 0.91, 0.94, std err = 9.99, 23..87, 0.0047; average error < 4cm^2
Thomas [67]	1998	Semi	67 F. 13 with Prader Willi.	Compared to bioelectrical impedance and anthropometry. Use standard measurement and 80% measurement for MRI	80% method had better performance against BIE and Anthro. MRI-BIE Bland-Altman LOA (+2% - 17%). MRI-Anthro Bland Altman LOA (-3% - 27%) with larger positive differences on for higher fat subjects.
Kamel [7]	1999	N	34 (17 male), 20-53y, non-obese	DEXA central abdominal fat, waist circumference, waist-to-hip Ratio	CAF and IAF correlation r=.83-.90.IAF by MRI and CAF by DEXA highly correlated. High correlations between IAF and WHR and waist circum in men
Gronemeyer [62]	2000	N	16 female, 19-44y	2 Manual techniques, one using thresholds other using region growing	Correlations SAT, VAT, TAT: r=.998,.885,.990; repeatability, pixel count differences: 0.2%,10.8%, 2.8%; means showed significant (student t) difference between two methods
Donnelly [48]	2003	Semi	Phantom: Simulated abdomen with cream and water	Compared measurements from 3 sequences: SE, Dixon, and 3D spoiled GE to ground truth	For all measurements, Dixon performed best followed by SE and then 3D spoiled GE.
Jin[87]	2003	Y	2 subjects, 6 slices per subject	Compared to "Ground truth" (average of 16 segmentations by 6 users) and "manual" (average of 3 segmentations)	Auto *vs.* "Ground Truth": True positive voxels ~92%. "Manual" *vs.* "Ground Truth": Area diffs of 2.0-4.1%. True positive voxels ~95%.
Poll [118]	2003	Semi	37, 48+/-13y,	Intra- and inter-observer reliability	Intra-observer reliability IAF, SCF and TAF: r = 0.999, r = 0.999 r = 1.0, observer II: r = 0.999, r = 0.999 and r = 1.0, inter-observer reliability IAF, SCF, and TAF: r = 0.999, r = 0.999, r = 1.0
Tintera [33]	2004	Semi	14, 25-35y, BMI>28	Water suppressed against standard turbo spin echo	Increase fat/muscle signal ratio by 4 times
Peng [35]	2005	Semi	6 (4F), 27-60y, BMI:20-38	Compared SNR and CNR for turbo SE and b-SSFP sequences	Turbo SE had better SNR for fat. Water saturated had better CNR for fat to muscle, small bowel and large bowel.
Peng [69]	2007	Yes	Phantom: Abdomen-like, vegetable oil	Compared accuracy of turbo SE and water saturated b-SSFP sequences against ground truth	Water saturated b-SSFP had better accuracy for all measurements, especially for internal oil.
Brennan [59]	2005	Y	42, including athletes	Compared BMI to body fat percentage and CAD BMI	'Reasonable' correlations between percentage, CAD BMI and BMI, but shortcomings of BMI were confirmed

(Table 3) Contd…

First Author	Year	Auto	Subject Data	Validation Technique	Results/Performance
Tatsuya [75]	2005	Semi	11 (9 female) healthy, Dixon,	Compared to single slice CT	No significant ($p<.05$ by student t-test) differences between CT and MR
Machann [68]	2005	Semi	80 (40 F) whole body scan	Reproducibility across same day scans	CV 1.2-1.8% for total tissue, 2.0%-2.7% for TAT, 3.1%-3.9% for VAT
Al-Attar [53]	2006	Semi	4 female: 1 FPLD2, 1 FPLD3, 2 C	Against anthropometry, inter/intra-observer correlations	Significant' differences among disease phenotypes. .985+ correlations for comparisons among observers
Armao [34]	2006	Semi	5 female	Compared 2 measurement techniques and 2 acquisition techniques: Water saturated (WS) and non-WS (NWS). Repeated measurements	Kappa = .8 for WS auto *vs*. manual; .2 for NWS auto *vs*. manual; .2 for WS *vs*. NWS. Among repeated measurements, SD of 2% for WS and 22% for NWS. High VAT errors when comparing NWS manual *vs*. auto, lower in WS.
Liou [70]	2006	Y	39 subjects. 15 slices each	Compared results from multiple pulse sequences to manual segmentations	Mean VAT error ranged from 0.1 to 1.6% sd from 1.6 to 2.9, r from 0.998 to 1 Mean VAT error ranged from -0.9 to 0% sd from 0.5 to 1.4, r from 0.999 to 1
Kullberg-Ahlström [54]	2007	Y	31 subjects. 13 datasets for derivation. 36 datasets from 18 subjects for validation.	Compared against 2 semi-automated measurements.	Errors (2.0±14%, -.84±2.7%) for (VAT,SAT). Mean TP:(90%, 96%), FP:(12±12%, 3.6%) for (VAT,SAT). Reproducibility: Auto (.24±7.1%, .21±2.3%); Semi 1 (2.2±12%, .61±4.2%); Semi 2 (4.7±11%,-2.5±3.4%) for (VAT,SAT).
Positano [74]	2008	Y	20 subjects, many corrupted	Compared to manual and Positano 04	Positano 04: CV (10.7,11.9,17.3%), r =(.97,.93,.95) (SAT, VAT,V/S). Positano 08: CV (9.8, 6.7, 13.1%), r=(.97,.99,.97) (SAT,VAT,V/S). B-A LOA '04 = -860-632cm^3; '08 -650 - 804 cm^3
Jørgensen [55]	2009	Y	14 male	Compare to manual. Correlations, Bland-Altman	Correlation r (SAT,VAT) = (.99,.96). B-A LOA SAT: -4.5% - 10.9%. VAT -7.2% - 27.4%
Kullberg [58]	2009	Y	24 (11 F). 12 overweight, 3 obese. Whole-body Dixon.	Compared against manual segmentation. Repeated acquisitions	CV = (2.0-2.7, 3.1-3.9%) for (TAT,VAT) for repeated acquisition. Mean CV for repeated measurements (2.32, 2.24, 1.01) for (VAT,SAT,TAT). VAT 7.6%FP, 11.3%FN. Bland-Altman
Kullberg [71]	2009	Semi	10 obese	Compared against DEXA and CT.	r >.975 for whole body MRI,CT,DEXA correlations. MRI overestimates SAT and underestimates VAT compared to CT
Sussman [52]	2010	Y	30	Compared to two manual raters	Bland-Altman plots *vs*. 2 manual observers

4.6. Table 3 Summary

Table **3** summarizes a few (39) reviewed papers regarding validation methods and the performance thus measured. Multiple sample sets included at least some overweight or obese patients. When subjects of only one sex were used, they were generally women. Multiple studies included athletes. The validation techniques used to evaluate the segmentation methods are diverse. Anthropometry, other imaging methods (like CT) and manual segmentation were the most commonly used comparators.

Many of the results obtained appear to indicate that these segmentation methods are at the very least close to being ready for clinical use. The validation statistics varied widely, but multiple automated methods performed nearly as well as manual ones. For example, Liou *et al.* found errors of less that 2% for visceral adipose tissue measurements and very few correlation coefficients between automated measurements and manual measurements were below 0.95.

5. APPLICATIONS

While the majority of the papers on the topic are devoted to simply measuring and identifying AT deposits, a few also integrate actual clinical applications. This section discusses some of the ways in which research scientists think their approaches can be applied in clinical practice.

5.1. Uses of Total AT Data

Though many articles cite a need for accurate measures of total body AT, the value of such accuracy is not clear since the associated diagnoses are simple to make without expensive and high tech equipment like an MRI. For exam-

ple, waist circumference correlates at 92% with MRI measures' total AT estimates and taken with other anthropometric measures, the correlation can be higher still [65].

For purposes other than diagnosis, especially for measuring change over time, the MRI can be an invaluable option. For example, Tintera *et al.* [33] used MRI to follow the changes in subjects' AT content after they began a lifestyle intervention to lose weight, and Barra *et al.* [102] made similar measurements of leg tissues during physical training. Whether the added precision of the MRI is worth the additional cost remains an open question.

Also, an automatic program that can measure total AT, and especially specific AT depots, could be useful for retrospective studies. This possibility is supported by Liou's findings, which indicated that different MR pulse sequences do not lead to statistically significant differences in manually-segmented AT volume [70]. It could also be possible for AT measurements to become routine for all abdominal MRI examinations. Both of these could yield data that indicates the risks associated with obesity.

5.2. Uses of AT Distribution Data

AT distribution data, may have diagnostic uses. For example, Al-Attar *et al*. [53] found that different kinds of metabolic syndrome have different distributions of AT to and within the legs, and Wajchenberg *et al.* [103] found similar differences in VAT and SAT, which means those distributions may be diagnostically useful. In fact, VAT content was measured with an MRI by Tanaka *et al.* [104] because the size of the visceral fat deposit is considered a diagnostic criterion for metabolic syndrome. Thomas *et al.* [105] found that MRI could be useful to monitor hepatic triglyceride content so as to direct interventions for Hepatic Steatosis. Chan *et al.* [106] explored the relationship between liver fat content and AT distribution, as well as other statistics. Fissoune *et al.* [107] used MRI to measure the changes in AT distribution of rats in a drug trial. Stevens *et al.* [108] explicated the already noted patterns in cardiovascular risk. Though Kvist's [109] group did manage to explain 94% and up of the variance in VAT using only two simple anthropometric measures, Kekes-Szabo *et al.* [110] conducted a similar study with less impressive results.

6. DISCUSSION

The discussion section consists of four parts. First we summarize what has been achieved so far: The state of the art. Then we discuss the role of image processing in AT measurement using MRI. Third, we identify a number of limitations and problems in the current investigation. Finally, we suggest new developments that can be expected in the coming years.

6.1. State of the Arts

Many approaches to MRI-based AT analysis have been proven reliable. Machann's study [68] on reproducibility is very thorough, with 80 people and high precision; the CV confidence interval is from 2-2.7% for total AT and from 3.1-3.9% for VAT. Elbers [85] had similar results. In fact, most of the papers reviewed provide confirmation of the value and precision of MRI-based measurements of AT.

A variety of special RF pulse sequences and analytical methods have proven effective. One such method is T1-weighting, which has overwhelmingly been shown to be effective. In fact, most of the papers reviewed in this article used some kind of T1-weighting. IR, an alternative RF pulse sequence, is used less, but also works well in identifying fat tissue [28, 36, 111].

One approach that may marginally reduce the amount of time required for MRIs is to use fewer scans. Fowler *et al.* [111] and Lancaster *et al.* [27] both explicitly tested the relevance of the number of slices. Lancaster *et al.* [27] found that no more than four were necessary, if the results were scaled. Thomas *et al.* [112] found that a test that used only one slice was generally effective in estimating changes in AT over time, and Shen *et al.* [113, 114] found that a single slice could be used to estimate VAT volume and its related health risks. However, Greenfield [115] found that single-slice CT was not reliable for absolute estimates due to inter-subject variation. Lee *et al.* [116] performed a further examination of the effects of inter-individual variation and found similar results. However, Liu *et al.* [50] found a predictive plane in which to measure the VAT of Chinese men.

Water suppression has been confirmed as a valuable tool. Tintera, Armao, Sobol and Tanaka's groups all showed that water suppression improves the accuracy of AT measurements [32-34, 36]. Tanaka *et al.* [36] compared two kinds of water suppression, and recommended a protocol using water suppression spectral pre-saturation with inversion recovery (WS-SPIR). Most of these methods depend on specific RF pulse sequences, so it is not possible to combine many of them.

The broad conclusion to be drawn from all of this recent work is that MRI is a powerful tool for fat analysis. All groups who made a comparison found that MRI performed as well as CT for all practical purposes [31, 32, 76, 117], though the two techniques had slight disagreements in the case of examining obese people. Abate *et al.*'s [63] study validated the MRI estimates by dissection, and found that the MRI estimates were very accurate. Fowler *et al.* [89] confirmed MRI against many anthropometric measures, and furthermore, found that all of the anthropometric measures (and their average) were individually closer to the MRI estimate than to one another. Kullberg *et al.*'s study and others also proved Dixon measures to be valuable tools in image analysis [39, 42, 46, 58].

MRI's accuracy with respect to AT measurements has been confirmed as roughly equivalent to CT's, except in obvious and long-familiar cases that involve metal implants and the like. This includes measurement of VAT and SAT, for which MRI has been shown to be reasonably accurate [54, 55, 58], especially when used in conjunction with water suppression, though difficulties in measuring VAT remain significant [60, 74].

6.2. Role of Image Processing

Much of the progress made in the field has been in image processing. Most importantly, image processing has enabled

development of the automated image analysis tools. These tools could dramatically improve the efficiency of image analysis. Also, by comparing the work of Sobol *et al.* [32] to that of Poll *et al.* [118], one can also see that image processing may improve reliability, though there are other relevant differences in that comparison. Image processing techniques also make it possible to quantify the amount of signal coming from individual voxels, which can be an important step in solving the partial volume problem [69].

There are some specific contextual advantages of certain methods of MRI scanning. For example, Liu *et al.* [50] argued that Dixon methods are favored to quantify fat in livers and other organs where AT is a smaller percent of each voxel. The approach of Peng *et al.* and others to use a gradient threshold allowed for inclusion of voxels with partial AT volume [69].

There are also differences among the currently developed automatic methods. Positano *et al.*'s [74] method depended on a snake algorithm that, depending on the (unclear) details of the constraints, could suffer from problems if used for patients with unusual abdominal shapes. Liou *et al.*'s [70] method appears to be more robust in such situations, but it is problematic that their automatically generated threshold was used in creating the validation set and may be sensitive to artifacts. Kullberg *et al.*'s [54] method also appears to perform well despite some variation in abdominal shape, but the algorithm did not perform well (in terms of percent error) on their leanest subjects. However, the performance of these algorithms on lean subjects may not be clinically significant, as such segmentations are unlikely to be necessary at all in such subjects.

Of all these automated methods, Liou *et al.*'s [70] performed the best, with higher correlations than Positano *et al.*'s [74] and similar error to Kullberg *et al.*'s [54] (Table **3**), but with lower variance in that error. Of course, this advantage might be partially explained by the use of the same automatically determined threshold for the manual segmentation; the determination of that threshold was not tested, though the rest of the algorithm performed well [70]. Still, the performance advantage of Liou *et al.*'s [70] method is marginal, and there may be strong reasons to favor of the other methods in different contexts.

There are a few commercial and research software packages available. All of the software packages examined by Bonekamp *et al.* [119] (HippoFat [74] by Positano's group, Analyze [120] by AnalyzeDirect, NIHImage [121] by the NIH, Slice-O-Matic [122] by Tomovision and EasyVision [123] by Phillips) generally performed well. NIHImage was rated as more difficult to use and less accurate than the others [121]. HippoFat [74] can be used as a fully automated method, as well as [124]. The specific effects of image-processing techniques on accuracy, a test of which would necessarily involve validation by a physically measured ground truth, are not entirely clear, since most of the phantom studies have compared combinations of MRI and image processing techniques. Still, valuable methods like Dixon imaging could not have been performed without advanced image processing techniques that deserve much of the credit for improvements in accuracy.

6.3. Limitations and Problems

One clear and nearly universal trend is that it is more difficult to measure VAT than it is to measure SAT. This result is confirmed in the studies by Gerard, Gronenmyer, Jørgensen and others [55, 62, 100].

The two major problems with MRI imaging are image artifacts and partial volume effects. These are connected, since partial volume effects are caused by low spatial resolution and image artifacts often worsen in the strong magnetic fields necessary for high resolution. One problem is that with increases in partial volume effects, the probability that VAT will be underestimated also increases [60]. Perhaps more importantly, the volume of intra- and inter-muscular adipose tissue, which can actually be comparable to VAT [125], can be underestimated. However, because AT depots tend to be large or of unclear significance to clinicians, the relevant error caused by partial volume effects is in most cases less concerning than the consequences of some image artifacts. Some have attempted to surmount the partial volume problem by estimating the amount of AT in a voxel by the intensity of the AT signal, such as Peng *et al.* This works best in images with very high contrast between AT and all other tissues, such as water-saturated tissues [69].

The adipose tissues within organs such as muscle and liver are important biomarkers that can be used to correlate with diseases. In order to quantify the adipose tissues in specific organs, the organs are often needed to be segmented or regions of interest be manually placed in the organ for measurement.

Although the methods in most clinical studies are somewhat validated against reference data from other measuring techniques, the lack of an ideal ground truth complicates the evaluation of the performance of clinical studies. Furthermore, since the methods and data used to acquire and validate segmentations are inconsistent across studies, it is difficult to directly compare results from different clinical studies. For example, except for a few of the methods reviewed in this paper, such as Liou *et al.*'s work [70] , all used some degree of user intervention, if not through manual segmentation, then through selection of parameters. Since it is difficult to know how broadly-applicable such manual modifications are, it is problematic to compare those methods to completely automatic ones.

7. FUTURE WORK TO BE DONE

From the perspective of public health, it may be best to have a publicly available and effective standard method for AT measurement and segmentation. Any standard method would rely on widely available software and hardware, or, if not currently so, then inexpensive at least. At that point, the standard could be tweaked in minor ways, but the narrow field of AT analysis using MRI could largely be considered a mastered one.

There are a variety of new techniques in development, for example rapid T2 Multi-Spin-Echo sequences [126]. Each of these techniques has only one or two papers devoted to it. These may eventually increase precision or accuracy, but the more basic and common methods may already perform well enough for most patients. It is possible that there

are or will be some contexts in which exceptional precision is needed, so these new ideas are still valuable, but they will not necessarily help most patients who need an AT MRI.

CONCLUSION

AT is not dynamic and there are relatively few structural complexities that need highly detailed analysis, so the requirements for AT measurement are considerably simpler than those warranted for something like brain imaging. T1-weighted imaging has been unequivocally confirmed as a valuable technique for most purposes. Image processing methods have improved accuracy and serve as the basis for many developing automated technologies. MRI-based measurement of VAT and SAT has been shown to be effective, though there are still improvements that need to be made in measuring VAT and AT measurement in specific organs. The primary challenge for the scientists of this review paper is to create functional algorithms and effective protocols that can be automated and distributed. The recent work presented above suggests that the field is rapidly approaching this goal.

LIST OF ABBREVIATIONS

ACM	=	Active Contour Modeling
AT	=	Adipose Tissue
BEI	=	Bioelectic Impedance
BMI	=	Body Mass Index
CAD	=	Computer-Assisted Diagnosis
CT	=	Computed Tomography
CV	=	Coefficient of Variation
DEXA	=	Dual Energy X-ray Absorptiometry
EM	=	Expectation-Maximization
FCM	=	Fuzzy-C Means
FP	=	False Positive
GE	=	Gradient Echo
IR	=	Inversion Recovery
LOA	=	Limits of Agreement
MR	=	Magnetic Resonance
MRI	=	Magnetic Resonance Imagining
N3	=	Non-parametric Non-uniform Intensity Normalization
NMR	=	Nuclear Magnetic Resonance
RF	=	Radio Frequency
ROI	=	Region of Interest
SAT	=	Subcutaneous AT
SE	=	Spin Echo
SNR	=	Signal to Noise Ratio
SSFP	=	Steady-State Free Precession
TAT	=	Total AT
TE	=	Echo Time
TI	=	Inversion Time
TP	=	True Positive
TR	=	Repeat Time
VAT	=	Visceral AT

CONSENT FOR PUBLICATION

Not applicable.

CONFLICT OF INTEREST

The authors declare no conflict of interest, financial or otherwise.

ACKNOWLEDGEMENTS

Declared none.

REFERENCES

[1] Preston S. Deadweight?-the influence of obesity on longevity. N Engl J Med 2005; 352: 1135-7.
[2] Pi-Sunyer F. Health implications of obesity. Am J Clin Nutr 1991; 53: 1595-603.
[3] Deckelbaum R, Williams C. Childhood obesity: The health issue. Obes Res 2001; 9: 239-43.
[4] McCargar L. New insights into body composition and health through imaging analysis. Can J Diet Pract Res 2007; 68: 160-5.
[5] Cefalu W, Werbel S, Bell-Farrow A, *et al*. Insulin resistance and fat patterning with aging: Relationship to metabolic risk factors for cardiovascular disease. Metabolism 1998; 47: 401-8.
[6] Gastaldelli A, Miyazaki Y, Pettiti M, *et al*. Metabolic effects of visceral fat accumulation in type 2 diabetes. J Clin Endocrinol Metab 2002; 87: 5098-103.
[7] Kamel E, McNeill G, Han T, *et al.* Measurement of abdominal fat by magnetic resonance imaging, dual-energy X-Ray absorbtiometry and anthropometry in non-obese men and women. Int J Obes Relat Metab Disord 1999; 23: 686-92.
[8] Mattsson S, Thomas B. Development of methods for body composition studies. Phys Med Biol 2006; 51: 203-28.
[9] Brambilla P, Bedogni G, Moreno L, *et al*. Crossvalidation of anthropometry against magnetic resonance imaging for the assessment of visceral and subcutaneous adipose tissue in children. Int J Obes (Lond) 2006; 30: 23-30.
[10] Keys A, Fidanza F, Karvonen M, Kimura N, Taylor H. Indices of relative weight and obesities. J Chronic Dis 1972; 25: 329-43.
[11] Nevill A, Stewart A, Olds T, Holder R. Relationship between adiposity and body size reveals limitations of BMI. Am J Phys Antrhopol 2006; 129: 151-6.
[12] Mazess R, Barden H, Bisek J, Hanson J. Dual-energy X-Ray absorbtiometry for total-body and regional bone-mineral and soft-tissue composition. Am J Clin Nutr 1990; 51: 1106-12.
[13] Borkan G, Gerzof S, Robbins A, Hults D, Silbert C, Silbert J. Assessment of abdominal fat content by computed tomography. Am J Clin Nutr 1982; 36: 172-7.
[14] Smith A, Parrish T, Abbott R, *et al.* Muscle-fat MRI: 1.5 Tesla and 3.0 Tesla versus histology. Muscle Nerve 2014; 50(2): 170-6.
[15] Reeder SB, Sirlin C. Quantification of liver fat with magnetic resonance imaging. Magn Reson Imaging Clin N Am 2010; 18(3): 337-57.
[16] Vovk U, Pernus F, Likar B. A review of methods for correction of intensity inhomogeneity in MRI. IEEE Trans Med Imaging 2007; 26: 405-21.
[17] van der Kooy K, Seidell J. Techniques for the measurement of visceral fat: A practical guide. Int J Obes Relat Metab Disord 1993; 17: 187-96.
[18] Hornak JP. The basics of MRI. Henietta, NY: Interactive learning software 2010.
[19] Rule GS, Hitchens TK. Fundamentals of protein NMR spectroscopy. Netherlands: Springer 2006.

[20] Damidian R. Tumor detection by nuclear magnetic resonance. Science 1971; 171: 1151-3.
[21] Lauterbur P. Image formation by induced local interactions: Examples employing nuclear magnetic resonance. Nature 1973; 242: 190-1.
[22] Mansfield P, Grannell P. NMR diffraction in solids. J Phys C: Solid State Phys 1973; 6: 422.
[23] Bottomley P, Foster T, Argersinger R, Pfeifer L. A review of normal tissue hydrogen NMR relaxation times and relaxation mechanisms: Dependence on tissue type, NMR frequency, temperature, species, excision, and age. Med Phys 1984; 11: 425-558.
[24] de Bazelaire C, Duhamel G, Rofsky N, Alsop D. MR imaging relaxation times of abdominal and pelvic tissues measured *in vivo* at 3.0 T: Preliminary results. Radiology 2004; 230: 652-9.
[25] Johnson G, Herfkens R, Brown M. Tissue relaxation time: *In vivo* field dependence. Radiology 1985; 156: 805-10.
[26] Dooms G, Hricak H, Margulis A, de Geer G. MR imaging of fat. Radiology 1986; 158: 51-4.
[27] Lancaster J, Ghiatas A, Alyassin A, Kilcoyne R, Bonora E, DeFronzo R. Measurement of abdominal fat with T1-weighted MR images. J Magn Reson Imag 1991; 1: 363-9.
[28] Barnard M, Schwieso J, Thomas E, *et al*. Development of a rapid and efficient magnetic resonance imaging technique for analysis of body fat distribution. NMR Biomed 1996; 9: 156-64.
[29] Terry J, Hinson W, Evans G, Schreiner P, Hagaman A, Crouse J. Evaluation of magnetic resonance imaging for quantification of intraabdominal fat in human beings by spin-echo and inversion-recovery protocols. Am J Clin Nutr 1995; 62: 297-301.
[30] Staten M, Totty W, Kohrt W. Measurement of fat distribution by magnetic resonance imaging. Invest Radiol 1989; 24: 345-9.
[31] Seidell J, Bakker C, van der Kooy K. Imaging techniques for measuring adipose-tissue distribution- a comparison between computed tomography and 1.5-T magnetic resonance. Am J Clin Nutr 1990; 51: 953-7.
[32] Sobol W, Rossner S, Hinson B, *et al*. Evaluation of a new magnetic resonance imaging method for quantitiating adipose tissue areas. Int J Obes (Lond) 1991; 15: 589-99.
[33] Tintera J, Harantova P, Cuchanek P, *et al*. Quantification of intra-abdominal fat during controlled weight reduction: Assessment Using the water-suppressed breath-hold MRI technique. Physiol Res 2004; 53: 229-34.
[34] Armao D, Guyon J, Firat Z, Brown M, Semelka R. Accurate quantification of visceral adipose tissue (VAT) using water-saturation mri and computer segmentation: Preliminary results. J Magn Reson Imag 2006; 23: 736-41.
[35] Peng Q, McColl R, Wang J, Chia J, Weatherall P. Water-saturated three-dimensional balanced steady-state free precession for fast abdominal fat quantification. J Magn Reson Imag 2005; 21: 263-71.
[36] Tanaka S, Yoshiyama M, Imanishi Y, *et al*. Measuring visceral fat with water-selective suppression methods (spir, spair) in patients with metabolic syndrome. Magn Reson Med Sci 2007; 6: 171-5.
[37] Li X, Youngren J, Hyun B, *et al*. Technical evaluation of *in vivo* abdominal fat and *IMCL* quantification using MRI and Mrsi at 3 T. Magn Reson Imag 2008; 26: 188-97.
[38] Dixon W. Simple proton spectroscopic imaging. Radiology 1984; 153: 189-94.
[39] Berglund J, Johansson L, Ahlstrom H, Kullberg J. Three-point dixon method enables whole-body water and fat imaging of obese subjects. Magn Reson Med Sci 2010; 63: 1659-68.
[40] Yeung H, Kormos D. Separation of true fat and water images by correcting magnetic field inhomogeneity *in situ*. Radiology 1986; 159: 783-6.
[41] Glover G, Schneider E. Three-point dixon technique for true water/fat decomposition with b0 inhomogeneity correction. Mag Reson Med 1991; 18: 371-83.
[42] Jingfei M. Dixon techniques for water and fat imaging. J Magn Reson Imag 2008; 28: 543-58.
[43] Kullberg J, von Below C, Lönn L, Lind L, Ahlstrom H, Johansson L. Practical approach for estimation of subcutaneous and visceral adipose tissue. Clin Phisiol Funct Imag 2007; 27: 148-53.
[44] Ma J, Wehrli F, Song H, Hwang S. A single-scan imaging technique for measurement of the relative concentrations of fat and water protons and their transverse relaxation times. J Magn Reson Imag 1997; 125: 92-101.
[45] Brix G, Heiland S, Bellemann M, Koch T, Lorenz W. MR imaging of fat-containing tissues: Valuation of two quantitative imaging techniques in comparison with localized proton spectroscopy. Magn Reson Imaging 1993; 11: 977-91.
[46] Moriguchi H, Lewin J, Durek J. Dixon techniques in spiral trajectories with off-resonance correction: A new approach for fat signal suppression without spatial-spectral RF pulses. Magn Reson Med 2003; 50: 915-24.
[47] Moriguchi H, Lewin J, Durek J. Fast spiral two-point dixon technique using block regional off-resonance correction. Magn Reson Med 2004; 52: 1342-50.
[48] Donnelly L, O'Brien K, Dardzinski B, *et al*. Using a phantom to compare mr techniques for determining the ratio of intraabdominal to subcutatneous adipose tissue. Am J Radiol 2003; 180: 993-8.
[49] Leinhard O, Johansson A, Rydell J, *et al,* Eds. Quantitative abdominal fat estimation using MRI. 19th International Conference on Pattern Recognition; 2008; Tampa, FL: IEEE 2009.
[50] Liu K, Chan Y, Chan J, Chan W, Kong M, Poon M. The preferred magnetic resonance imaging planes in quantifying visceral adipose tissue and evaluating cardiovascular risk. Diabetes Obes Metab 2005; 7: 547-54.
[51] Yu H, Reeder S, Shimakawa A, Brittain J, Pelc N. Field map estimation with a region-growing scheme for iterative 3-point water-fat decomposition. Magn Reson Med 2005; 54: 1032-9.
[52] Sussman D, Yao J, Summers R. Automated fat measurement and segmentation with intensity inhomogeneity correction. SPIE Med Imag 2010; doi: 10.1117/12.843860.
[53] Al-Attar S, Pollex R, Robinson J, *et al*. Semi-automated segmentation and quantification of adipose tissue in calf and thigh by MRI: A preliminary study in patients with monogenic metabolic syndrome. BMC Med Imag 2006; 6: 11.
[54] Kullberg J, Ahlstrom H, Johansson L, Frimmel H. Automated and reproducible segmentation of visceral and subcutaneous adipose tissue from abdominal MRI. Int J Obes (Lond) 2007; 31: 1806-17.
[55] Jørgensen P, Larsen R, Wraae K, Eds. Unsupervised assessment of subcutaneous and visceral fat by MRI. SC IA 2009; 5575: 179-88.
[56] Sled J, Zijdenbos A, Evans A. A nonparametric method for automatic correction of intensity nonuniformity in MRI data. IEEE Trans Med Imag 1998; 17: 87-97.
[57] Tustison N, Gee J. N4ITK: Nick's N3 ITK implementation for MRI bias field correction. Insight J 2009: 640.
[58] Kullberg J, Johansson L, Ahlstrom H, *et al*. Automated assessment of whole-body adipose tissue depots from continuously moving bed MRI: A feasibility study. J Magn Reson Imag 2009; 30: 185-93.
[59] Brennan D, Whelan P, Robinson K, *et al*. Rapid automated measurement of body fat distribution from whole-body MRI. Am J Radiol 2005; 185: 418-23.
[60] Positano V, Gastaldelli A, Sironi A, Santarelli M, Lombardi M, Landini L. An accurate and robust method for unsupervised assessment of abdominal fat by MRI. J Magn Reson Imaging 2004; 20: 684-9.
[61] Glasbey C, Young M. Maximum a posteriori estimation of image boundaries by dynamic programming. Appl Stat 2002; 51: 209-21.
[62] Gronenmeyer S, Steen R, Kauffman W, Reddick W, Jo G. Fast Adipose Tissue (FAT) assessment by MRI. Magn Reson Imag 2000; 18: 815-18.
[63] Abate N, Burns D, Peshock R, Garg A, Grundy S. Estimation of AT mass by magnetic resonance imaging: Validation against dissection in human cadavers. J Lipid Res 1994; 35: 1490-6.
[64] Han T, McNeill G, Seidell J, Lean M. Predicting intra-abdominal fatness from anthropometric measures: The influence of stature. Int J Obes 1997; 21: 587-93.
[65] Ross R, Leger L, Guardo R, de Guise J, Pike B. Adipose tissue volume measured by magnetic resonance imaging and computerized tomography in rats. J Appl Physiol 1992; 70: 2164-72.
[66] Han T, Kelly I, Walsh K, Greene R, Lean M. Relationship between volumes and areas from single transverse scans of intra-abdominal fat measured by magnetic resonance imaging. Int J Obes 1997; 21: 1161-6.
[67] Thomas E, Saeed N, Hajnal J, *et al*. Magnetic resonance imaging of total body fat. J Appl Physiol 1998; 85: 1778-85.
[68] Machann J, Thamer C, Schnoedt B, *et al*. Standardized assessment of whole body adipose tissue topography by MRI. J Magn Reson Imag 2005; 21: 455-62.
[69] Peng Q, McColl R, Ding Y, Wang J, Cia J, Weatherall P. Automated method for accurate abdominal fat quantification on water-saturated magnetic resonance images. J Magn Reson Imag 2007; 26: 738-46.

[70] Liou T, Chan W, Pan L, Lin P, Chou P, Chen C. Fully automated large-scale assessment of visceral and subcutaneous abdominal adipose tissue by Magnetic Resonance Imaging. Int J Obes 2006; 30: 844-52.

[71] Kullberg J, Brandberg J, Angelhed J, *et al.* Whole-body adipose tissue analysis: Comparison of MRI, CT and dual energy X-Ray absorptiometry. Br J Radiol 2009; 974: 123-30.

[72] Otsu N. A threshold selection method from gray-level histograms. IEEE Trans Syst Man Cybern 1979; 9: 62-6.

[73] Poll W, Wittsack H, Koch J, *et al.* Quantification of total abdominal fat volumes using magnetic resonance imaging. Eur J Med Res 2002; 7: 347-52.

[74] Positano V, Cusi K, Santarelli M, *et al.* Automatic correction of intensity inhomogeneities improves unsupervised assessment of abdominal fat by MRI. J Magn Reson Imaging 2008; 28: 403-10.

[75] Tatsuya G, Kawawa Y, Nagamoto M, Terada H, Kohda E. Measurement of visceral fat/subcutaneous fat ratio by 0.3 Tesla MRI. Radiat Med 2005; 23: 584-87.

[76] He L, Peng Z, Everding B, *et al*. A comparative study of deformable contour methods on medical image segmentation. Imag Vis Comp 2008; 26: 141-63.

[77] Kass M, Andrew W, Demetri T. Snakes: Active contour models. Int J Comp Vis 1988; 1: 321-31.

[78] Cohen L, Cohen I. Finite-element methods for active contour models and balloons for 2-D and 3-D images. IEEE Trans Pattern Analysis Machine Intelligence 1993; 15: 1131-47.

[79] Hamarneh G, Yang J, McIntosh C, Langille M. 3D live-wire-based semi-automatic segmentation of medical images. SPIE Med Imag 2005; 5747: doi: 10.1117/12.596148 .

[80] Glasbey C, Young M. Maximum a posteriori estimation of image boundaries by dynamic programming. Appl Stat 2002; 51: 209-21.

[81] Freedman D, Zhang T. Interactive graph cut based segmentation with shape priors. IEEE Comp Soc Conf Comp Vision Pattern Recogn 2005; 1: 755-62.

[82] Mitchell S, Bosch J, Lelieveldt B, van der Geest R, Reiber J, Sonka M. 3Dactive appearance models: Segmentation of cardiac MR and ultrasound images. IEEE Trans Med Imaging 2002; 21: 1167-78.

[83] Heimann T, Meinzer H-P. Statistical shape models for 3D medical image segmentation: A review. Medical Image Analysis 2009; 13(4): 543-63.

[84] Wang H, Suh JW, Das SR, Pluta JB, Craige C, Yushkevich PA. Multi-atlas segmentation with joint label fusion. IEEE Trans Patt Anal Mach Intelli 2013; 35(3): 611-23.

[85] Elbers J, Haumann G, Assecheman H, Seidell J, Gooren L. Reproducibility of fat area measurements in young, non-obese subjects by computerized analysis of Magnetic Resonance Images. Int J Obes 1997; 21: 1121-9.

[86] Udupa J, Saha P, Lotufo R. Relative fuzzy connectedness and object definition: theory, algorithms and applications in image segmentation. IEEE Trans Patt Anal Mach Intelli 2002; 24: 1485-500.

[87] Jin Y, Imielinska CZ, Laine AF, Udupa J, Shen W, Heymsfield SB. Segmentation and evaluation of adipose tissue from whole body MRI scans. MICCAI 2003; 2878: 635-42.

[88] Roullier V, Cavaro-Menard C, Calmon G, Aube C. Fuzzy algorithms: Application to adipose tissue quantification on MR images. Biomed Signal Process Cont 2007; 2: 239-47.

[89] Fowler P, Fuller M, Glasbey C, *et al*. Total and subcutaneous adipose tissue in women: The measurement of distribution and accurate prediction of quantity by using Magnetic Resonance Imaging. Am J Clin Nutr 1991; 54: 18-25.

[90] Shen W, Wang Z, Tang H, *et al.* Volume estimates derived *in vivo* by imaging methods: Model comparisons with visible woman as the reference. Obes Res 2003; 11(2): 217-25.

[91] Martin A, Daniel M, Drinkwater D, Clarys J. Adipose tissue density, estimated adipose lipid fraction and whole body adiposity in male cadavers. Int J Obes Relat Metab Disord 1994; 18: 79-83.

[92] Frederick E, Cowden D, Klein S. Applied General Statistics. 3rd ed. Englewood Cliffs, N. J.: Prentice Hall 1967.

[93] Myers J, Well AD. Research design and statistical analysis. 2nd ed. Mahwah, NJ: Lawrence Erlbaum Associates 2003.

[94] Altman D, Bland J. Measurement in medicine: The analysis of method comparison studies. The Statistician 1983; 32: 307-17.

[95] Yoon D, Moon J, Kim H, *et al.* Comparison of low-dose ct and mr for measurement of intra-abdominal adipose tissue: A phantom and human study. Acad Radiol 2008; 15: 62-70.

[96] McNeill G, Fowler P, Maughan R, *et al.* Body Fat in lean and overweight women estimated by six methods. Br J Nutr 1991; 65: 95-103.

[97] Aristizabal J, Restrepo M, Amalia L. Validation by hydrodensitometry of skinfold thickness equations used for female body composition assessment. Biomedica 2008; 28: 404-13.

[98] Ward L, Cornish B, Fuller N, Dewit O, Elia M, Thomas B, Eds. Bioelectrical impedance analysis: The electronic skin-fold caliper? 2nd International Conference on Bioelectromagnetism; 1998. Melbourne : IEEE 2002

[99] Yoneda M, Tasaki H, Tsuchiya N, *et al.* A study of bioelectrical impedance analysis methods for practical visceral fat estimation. IEEE International Conference on Granular Computing; 2007. Fremont: IEEE 2007.

[100] Gerard E, Snow R, Kennedy D, *et al*. Overall body fat and regional fat distribution in young women: Quantification with MR imaging. Am J Radiol 1991; 157: 99-104.

[101] Srdic B, Stokic E, Polzovic A, Babovic S. Abdominal adipose tissue-significance and methods of detection. Med Pregl 2005; 58: 258-64.

[102] Barra V, Morio B, Colin A, Vermorel M, Boire J. Automatic assessment of muscle/fat temporal variations on MR images of the thigh. 18th Annual International Conference of Engineering in Medicine and Biology Society; 1996. Amsterdam: IEEE 2002.

[103] Wajchenberg B. Subcutaneous and visceral adipose tissue: Their relation to the metabolic syndrome. Endocr Rev 2000; 21: 697-738.

[104] Tanaka S, Yoshiyama M, Imanishi Y, *et al.* MR measurement of visceral fat: Assessment of metabolic syndrome. Magn Reson Med Sci 2006; 5: 207-10.

[105] Thomas E, Hamilton G, Patel N, *et al*. Hepatic triglyceride content and its relation to body adiposity: A magnetic resonance imaging and proton magnetic resonance spectroscopy study. Gut 2005; 54: 122-7.

[106] Chan D, Watts G, Ng T, Hua J, Song S, Ph B. Measurement of liver fat by magnetic resonance imaging: Relationships with body fat distribution, insulin sensitivity and plasma lipids in healthy men. Diabetes Obes Metab 2006; 8: 698-702.

[107] Fissoune R, Pellet N, Chaabane L, Contard F, Guerrier D, Briguet A. Evaluation of adipose tissue distribution in obese Fa/Fa Zucker Rats by *in vivo* MR imaging: Effects of peroxisome proliferator-activated receptor agonists. Magma 2004; 17: 229-35.

[108] Stevens J. Obesity, fat patterning and cardiovascular risk. Adv Exp Med Biol 1995; 369: 21-7.

[109] Kvist H, Chowdhury B, Grangard U, Tylen U, Sjostrom L. Total and visceral adipose-tissue volumes derived from measurements with computed tomography in adult men and women: Predictive equations. Am J Clin Nutr 1988; 48: 1351-61.

[110] Kekes-Szabo T, Hunter G, Nyikos I, Williams M, Blaudeau T, Snyder S. Anthropometric equations for estimating abdominal adipose tissue distribution in women. Int J Obes Relat Metab Disord 1996; 20: 753-8.

[111] Fowler P, Knight C, Cameron G, Foster M. Use of magnetic resonance imaging in the study of goat mammary glands *in vivo*. J Reprod Fert 1990; 89: 359-66.

[112] Thomas E, Bell J. Influence of undersampling on magnetic resonance imaging measurements of intra-abdominal adipose tissue. Int J Obes Relat Metab Disord 2003; 27: 211-8.

[113] Shen W, Punyanitya M, Chen J, *et al.* Visceral adipose tissue: Relationships between single slice areas at different locations and obesity-related health risks. Int J Obes (Lond) 2007; 31(5): 763-9.

[114] Shen W, Punyanitya M, Wang Z, *et al.* Visceral adipose tissue: Relations between single-slice areas and total volume. Am J Clin Nutr 2004; 80(2): 271-8.

[115] Greenfield J, Samaras K, Chisholm D, Campbell L. Regional intrasubject variability in abdominal adiposity limits usefulness of computed tomography. Obes Res 2002; 10: 260-5.

[116] Lee S, Janssen I, Ross R. Interindividual variation in abdominal subcutaneous and visceral adipose tissue: Influence of measurement site. J Appl Physiol 2004; 97: 948-54.

[117] Positano V, Christiansen T, Santarelli M, Ringgaard S, Landini L, Gastaldelli A. Accurate segmentation of subcutaneous and intermuscular adipose tissue from MR images of the thigh. J Magn Res Imag 2009; 29: 377-684.

[118] Poll W, Wittsack H, Koch J, *et al.* A rapid and reliable semiautomated method for measurement of total abdominal fat volumes us-

ing magnetic resonance imaging. Magn Reson Imag 2003; 21: 631-6.

[119] Bonekamp S, Ghosh P, Crawford S, *et al*. Quantitative comparison and evaluation of software packages for assessment of abdominal adipose tissue distribution by Magnetic Resonance Imaging. Int J Obes (Lond) 2008; 32: 100-11.

[120] AnalyzeDirect. Analyze 10.0 http://www.analyzedirect.com/Analyze/default.asp. Available at: http://www.analyzedirect.com/Analyze/default.asp.

[121] NIH. NIHImage. Available at: http://rsbweb.nih.gov/nih-image/.

[122] Tomovision. SliceOmatic. Available at: http://www.tomovision.com/products/sliceomatic.htm.

[123] Phillips. EasyVision and EasyScil. Available at: http://www.bmi2.bmt.tue.nl/image-analysis/Research/Software/EasyScil/.

[124] Arif H, Racette S, Villareal S, Holloszy J, Weiss E. Comparison of methods for assessing abdominal adipose tissue from Magnetic Resonance Images. Obesity 2007; 15: 2240-4.

[125] Gallagher D, Kuznia P, Heshka S, *et al.* Adipose tissue in muscle: A novel depot similar in size to visceral adipose tissue. Am J Clin Nutr 2005; 81(4): 903-10.

[126] Gensanne D, Josse G, Theunis J, Lagarde J, Vincensini D. Quantitate Magnetic Resonance Imaging of subcutaneous adipose tissue. Skin Res Tech 2009; 15: 45-50.

[127] Kullberg J, Angelhed J, Lönn L, *et al.* Whole-body T1 mapping improves the definition of adipose tissue: Consequences for automated image analysis. J Magn Reson Imaging 2006; 24: 395-401.

[128] Demerath E, Shen W, Lee M, *et al*. Approximation of total visceral adipose tissue with a single Magnetic Resonance Image. Am J Clin Nutr 2007; 85(2): 362-8.

[129] Ohsuzu F, Kosuda S, Takayama E, *et al.* Imaging techniques for measuring adipose-tissue distribution in the abdomen: A comparison between computed tomography and 1.5-Tesla magnetic resonance spin-echo imaging. Radiation Medicine 1998; 16: 99-107.